



UNIVERSITÀ  
DEGLI STUDI  
FIRENZE

## FLORE

# Repository istituzionale dell'Università degli Studi di Firenze

### **Upper mantle structure of the southern Arabian margin: Insights from teleseismic tomography**

Questa è la Versione finale referata (Post print/Accepted manuscript) della seguente pubblicazione:

*Original Citation:*

Upper mantle structure of the southern Arabian margin: Insights from teleseismic tomography / Korostelev, F., Leroy, S., Keir, D., Ahmed, A., Boschi, L., Rolandone, F., Stuart, G. W., Obrebski, M., Khanbari, K., El-Hussain, I.. - In: GEOSPHERE. - ISSN 1553-040X. - ELETTRONICO. - 11:(2015), pp. 1262-1278. [10.1130/GES01159.1]

*Availability:*

This version is available at: 2158/1077602 since: 2020-10-28T16:30:15Z

*Published version:*

DOI: 10.1130/GES01159.1

*Terms of use:*

Open Access

La pubblicazione è resa disponibile sotto le norme e i termini della licenza di deposito, secondo quanto stabilito dalla Policy per l'accesso aperto dell'Università degli Studi di Firenze (<https://www.sba.unifi.it/upload/policy-oa-2016-1.pdf>)

*Publisher copyright claim:*

(Article begins on next page)

## GEOSPHERE

GEOSPHERE; v. 11, no. 5

doi:10.1130/GES01159.1

11 figures

CORRESPONDENCE: felicie.korostelev@gmail.com

CITATION: Korostelev, F., Leroy, S., Keir, D., Ahmed, A., Boschi, L., Rolandone, F., Stuart, G.W., Obrebski, M., Khanbari, K., and El-Hussain, I., 2015, Upper mantle structure of the southern Arabian margin: Insights from teleseismic tomography: *Geosphere*, v. 11, no. 5, p. 1262–1278, doi:10.1130/GES01159.1.

Received 28 November 2014

Revision received 16 July 2015

Accepted 12 August 2015

Published online 15 September 2015



This paper is published under the terms of the CC-BY license.

© 2015 Geological Society of America

# Upper mantle structure of the southern Arabian margin: Insights from teleseismic tomography

Félicie Korostelev<sup>1,\*</sup>, Sylvie Leroy<sup>1,\*</sup>, Derek Keir<sup>2,\*</sup>, Abdulhakim Ahmed<sup>1,3,\*</sup>, Lapo Boschi<sup>1,\*</sup>, Frédérique Rolandone<sup>1,\*</sup>, Graham W. Stuart<sup>4,\*</sup>, Mathias Obrebski<sup>1,\*</sup>, Khaled Khanbari<sup>5,\*</sup>, and Issa El-Hussain<sup>6,\*</sup>

<sup>1</sup>Sorbonne Universités, UPMC (Université Pierre et Marie Curie) Université Paris 06, CNRS (Centre National de la Recherche Scientifique), Institut des Sciences de la Terre de Paris (iSTeP), 4 place Jussieu, 75005 Paris, France

<sup>2</sup>National Oceanography Centre Southampton, University of Southampton, Waterfront Campus, European Way, Southampton SO14 3ZH, UK

<sup>3</sup>Seismological and Volcanological Observatory Center, Dharmar, Yemen

<sup>4</sup>School of Earth and Environment, University of Leeds, Maths/Earth and Environment Building, Leeds LS2 9JT, UK

<sup>5</sup>Sana'a University, Yemen Remote Sensing and GIS Center, Sana'a, Yemen

<sup>6</sup>Earthquake Monitoring Center, University of Sultan Qaboos, P.C. 213 Muscat, Oman

## ABSTRACT

We image the lithospheric and upper asthenospheric structure beneath the central and eastern parts of the northern Gulf of Aden rifted passive continental margin with 59 broadband stations to evaluate the role of transform fault zones on the evolution of magma-poor continental margins. We used teleseismic tomography to compute a relative P wave velocity model in eastern Yemen and southern Oman down to 400 km depth. Our model shows low-velocity anomalies located in the vicinities of five major fracture zones and regions of recent volcanism. These low-velocity anomalies are likely caused by localized asthenospheric upwelling and partial melting, caused by small-scale convection promoted by gradients in the lithosphere-asthenosphere boundary topography near the fracture zones. In addition, low velocities underlie regions of elevated topography between major sedimentary basins. We suggest that locally buoyant mantle creates uplift and dynamic topography on the rift margin that affects the course of seasonal rivers and the sedimentation at the mouth of those rivers. Our new P wave velocity model suggests that the dynamic topography and recent volcanism in the central and eastern Gulf of Aden could be due to small-scale convection at the edge of the Arabian plate and/or in the vicinity of fracture zones.

## INTRODUCTION

There are two main categories of passive continental margins: volcanic margins where there is evidence of significant magmatism, or magma poor where there is not. If magmatism is present, it may be synbreakup or post-breakup. Explanations for magmatism during breakup include rifting above

\*Emails: Korostelev: felicie.korostelev@gmail.com; Leroy: sylvie.leroy@upmc.fr; Keir: D.Keir@soton.ac.uk; Ahmed: hakim66@myself.com; Boschi: lapo.boschi@upmc.fr; Rolandone: frederique.rolandone@upmc.fr; Stuart: G.W.Stuart@leeds.ac.uk; Khanbari: kkhannbari@hotmail.com; El-Hussain: elhussain@squ.edu.om

mantle with elevated temperatures (White et al., 2008) or more than normal volatile component (Shillington et al., 2009), which promote greater melting. Abnormal mantle temperatures are commonly attributed to presence of a mantle plume beneath a rift (e.g., Debayle et al., 2001; Chang et al., 2011), or from lateral flow and channelization of plume material along thinned lithosphere (e.g., Ebinger and Sleep, 1998; Leroy et al., 2010b). Mantle melting can also be promoted by elevated rates of plate thinning, achieved either by faster or more localized extension (White and McKenzie, 1989; Bown and White, 1995; Bastow and Keir, 2011). Increased melting can also be caused by presence of localized thin zones in the plate prior to arrival of a thermal anomaly and extension (Armitage et al., 2010). Models predict that the thermal anomaly created by synrift mantle upwelling will cool after breakup. For the Gulf of Aden, we expect the mantle to have cooled by 50 °C since breakup ~18 m.y. ago (Lucas et al., 2008), and therefore no magmatism is expected. Causes of magmatism both during and after continental rifting include small-scale convection (e.g., King and Anderson, 1998; Morency et al., 2005) and melt focusing (Kendall et al., 2005), both caused by sharp gradients in the lithosphere-asthenosphere boundary topography. In the central and eastern Gulf of Aden postrift magmatism exposed at the surface is localized spatially (Fig. 1) and associated with the termination of major fracture zones (Figs. 1 and 2). In this paper we image the seismic velocity structure of the mantle beneath the central and eastern Gulf of Aden in order to understand the mantle processes responsible for their origin.

The Gulf of Aden provides a unique opportunity to study how magmatism affects the breakup process as the passive continental margin transitions in character from nonvolcanic in the east to volcanic in the west. The transition is most commonly attributed to elevated mantle potential temperatures of 1450 K during breakup in the west (Rooney et al., 2012; Ferguson et al., 2013) compared to normal mantle potential temperatures in the east. Elevated mantle temperatures in the west are likely caused by presence of the deep-seated plume (e.g., Debayle et al., 2001; Bastow et al., 2008). The Gulf of Aden has conjugate rifted continental margins that are 50–250 km apart in the magma-rich west,

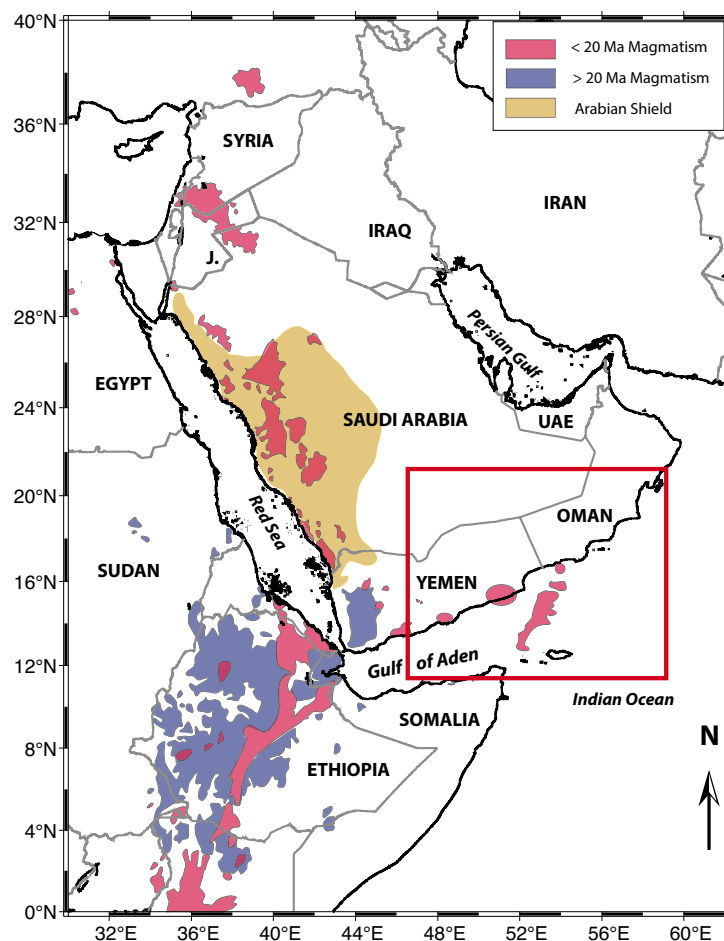


Figure 1. Map of volcanism in Arabia; red box indicates study area (the eastern Gulf of Aden). J.—Jordan, UAE—United Arab Emirates.

increasing to 500 km apart in the magma-poor east. Some localized patches of surface volcanism have been observed on the magma-poor margin of the central and eastern Gulf of Aden (Figs. 1 and 2). These two types of passive continental margins are well studied, but the transition from one to the other is not well known. We study the structure of the lithosphere and upper asthenospheric mantle under the northern Gulf of Aden passive continental margin from the city of Al Mukalla (49°E, 14.5°N, Yemen) to Ras Madrakah (58°E, 19°N, Oman), within which the margin is segmented along strike by five major transform fracture zones (Fig. 2). We use our imaging of mantle structure and its

spatial relationship to volcanism and major structures such as fracture zones to understand the origins of the magmatism after breakup.

Our work incorporates data from 32 broadband stations in Yemen and 27 broadband stations in the southern Sultanate of Oman (Dhofar region: Leroy et al., 2010a; Ahmed et al., 2013; Korostelev et al., 2014; Corbeau et al., 2014) that operated during the 2009–2011 YOCMAL project (young conjugate margins laboratory) (Fig. 2). In addition, we used the recordings from 30 broadband stations from the 2003–2006 Dhofar Seismic Experiment (in Oman; Basuyau et al., 2010; Fig. 2). In total we incorporate 833 earthquakes recorded from 2003 to 2006 and from 2009 to 2011 (Fig. 3) to compute a velocity model for the propagation of P waves in the crust and upper part of the mantle. To do that, we used the classical ACH teleseismic tomography method (Aki et al., 1974). This method consists of embedding a local three-dimensional model volume that is beneath the network within a global spherically symmetric reference model. The ACH method is used together with the fast marching method (FMM) (e.g., Sethian 1996, 1999, 2001) that rapidly computes traveltimes into the model. We aim to characterize the lithospheric and upper asthenospheric structures of the passive continental margin of the eastern Gulf of Aden in order to (1) demonstrate the influence of major transform faults on the passive continental margins, and (2) provide a better understanding of the origin of surface volcanoes and topography.

## GEODYNAMIC SETTING

The continental rifting of the Gulf of Aden began ca. 34 Ma (Robinet et al., 2013); seafloor spreading initiated at the beginning of Miocene, 17.6 Ma (d'Acremont et al., 2006, 2010; Leroy et al., 2012). During the same period, mantle exhumation was activated east of the Alula-Fartak fracture zone (d'Acremont et al., 2006; Leroy et al., 2010a; Autin et al., 2010; Watremez et al., 2011). Extension proceeded in a west-southwest direction as far as the Gulf of Tadjoura. The Gulf of Aden extension direction is oblique to the strike of the rift, resulting in it being segmented by several major fracture zones striking N020°–N030° (Fig. 2).

The Gulf of Aden has a magma-poor or nonvolcanic margin to the east (Leroy et al., 2004; d'Acremont et al., 2005) and a magma-rich or volcanic margin to the west (Tard et al., 1991; Leroy et al., 2012; Ahmed et al., 2013); the magmatism is commonly attributed to elevated mantle temperatures associated with a mantle plume beneath Afar. It was previously assumed that the major discontinuity of Shukra el Sheik (long ~44°E) may indicate the spatial limit of the Afar plume's influence, as it corresponds to a major change in rheology of the lithosphere (Hébert et al., 2001). However, several studies propose a limit of influence up to Xiis–Al Mukalla fracture zone (e.g., Leroy et al., 2012; Bellahsen et al., 2013). The rifted continental volcanic margins near the plume have synrift seaward-dipping reflector sequences to 5 km thick (Tard et al., 1991; Leroy et al., 2012). Seaward-dipping reflectors are sparse in the east, especially in the ocean-continent transition (Autin et al., 2010; Leroy et al., 2010a), and no synrift volcanism has been observed east of long 46°E (Leroy et al., 2012; see Figs. 1 and 2).



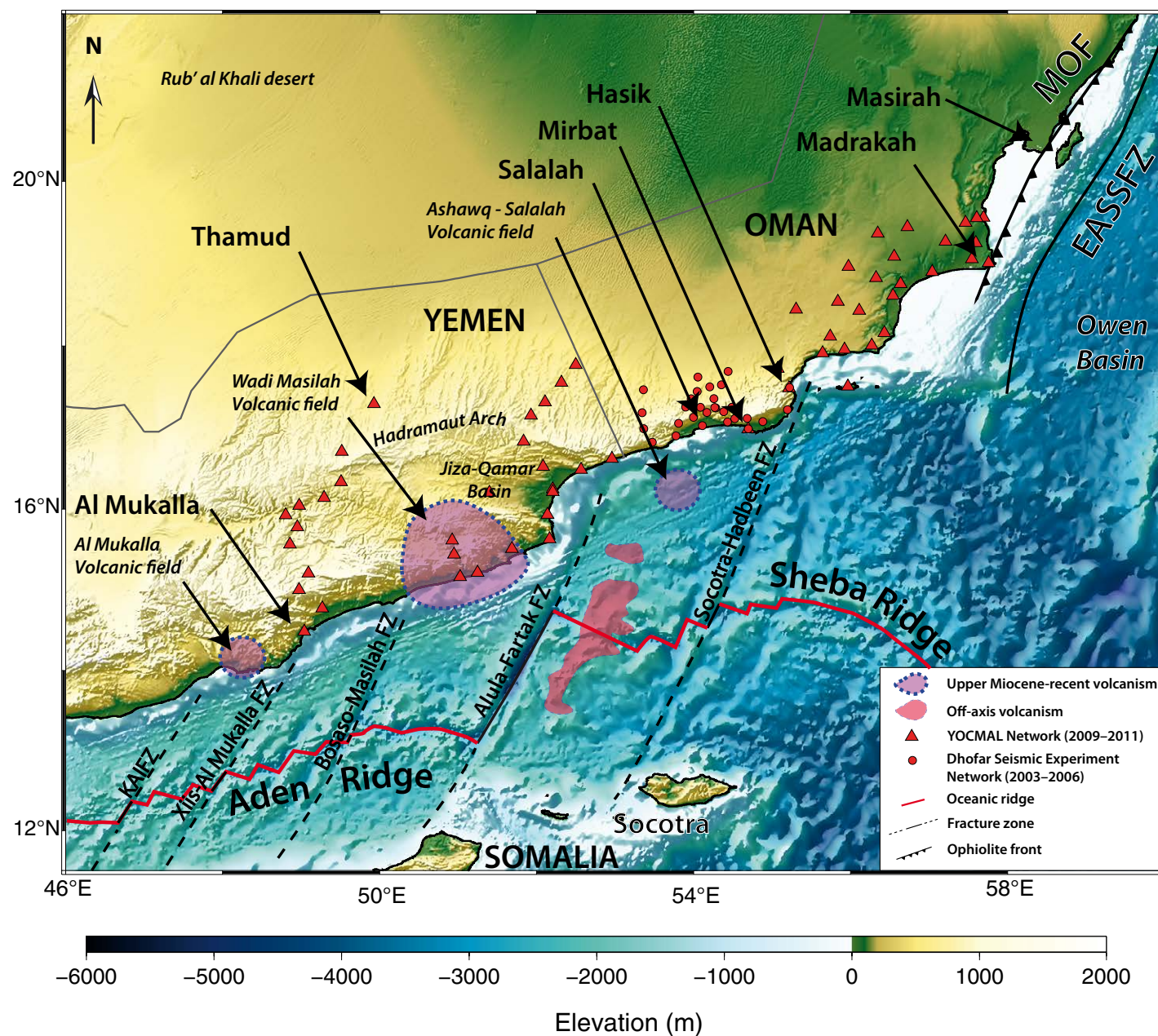


Figure 2. Geodynamic map of the eastern Gulf of Aden. KAIFZ—Khanshir Al Irqah fracture zone (FZ); EASSFZ—East Arabian strike-slip fault zone; MOF—Masirah ophiolite front; YOCMAL—young conjugate margins laboratory (see text).

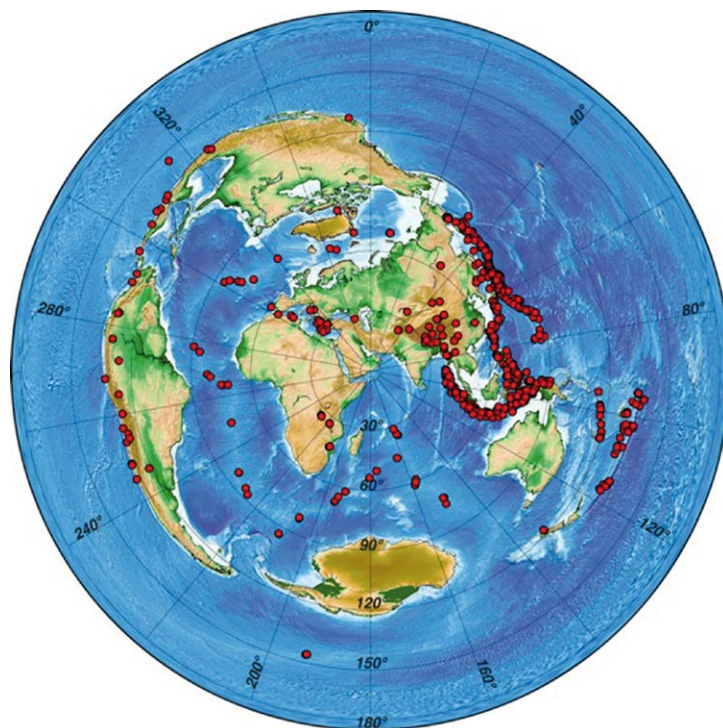


Figure 3. Azimuthal distribution of earthquakes of magnitude 5.5 or more used in this study.

We studied the eastern part of Yemen and southwestern part of Oman in a region from the city of Al Mukalla (49°E, 14.5°N, Yemen) to Ras Madrasah (58°E, 19°N, Oman) (Fig. 2). The study region includes the landward continuation of five main fracture zones that can be mapped at sea, oriented N025°–N030°, the Khanshir Al Irqah, Xiis–Al Mukalla, Bosaso–Masilah, Alula–Fartak, and Socotra–Hadbeen fracture zones (Leroy et al., 2012; Bellahsen et al., 2013). The most striking geological pattern of the area is the presence of recent volcanism near the city of Al Mukalla (49°E, 14.5°N, Yemen), and around the southern part of Wadi Masilah (Leroy et al., 2010a; purple shaded areas, Fig. 2). Other volcanic fields exist on the southern conjugate margin in Somalia, near Bosaso and Qandala (Fantozzi and Sgavetti, 1998). Moreover, some recent magmatism has been observed offshore in the ocean-continent transition of the eastern Gulf of Aden margin (Lucazeau et al., 2009; Autin et al., 2010; Watremez et al., 2011), offset from the axis of the Sheba ridge (d'Acremont et al., 2010) and below the adjoining continental margin in the north (Basuyau et al., 2010).

The Gulf of Aden oceanic basin is located between two 150-km-thick blocks of continental lithosphere (Rolandone et al., 2013), and has a configuration that promotes channelization of plume material from Afar to the east, along

the Aden and Sheba ridges (Leroy et al., 2010b). It has been proposed that the 180 km offset of the Alula–Fartak fracture zone (d'Acremont et al., 2010) limits the flow, causing part of the plume material to be redirected between the Alula–Fartak and the Socotra–Hadbeen fracture zones (Fig. 2).

In the easternmost part of our study zone, the East Arabian strike-slip fault zone is a north-northwest fault zone offshore Ras Madrasah (58°E, 19°N) and Masirah Island (58.5°E, 20.5°N, Fig. 2). This strike-slip fault is located between two different units: the Masirah ophiolite (obducted oceanic crust of Tithonian age) and the Owen basin (oceanic crust of Cenozoic age) (Immenhauser, 1996; Whitmarsh, 1979; Prell et al., 1990; Robinet et al., 2013). The Masirah ophiolite front is the contact zone between continental units of the Masirah basin to the west and the Masirah ophiolite to the east (Fig. 2).

## PREVIOUS SEISMOLOGIC STUDIES

Several seismological studies were conducted on the Arabian plate during the past few decades. They enable us to better understand the seismic structure of the crust and the lithosphere, thereby constraining the morphology and elastic properties of the Arabian plate, from which its evolution can be interpreted (e.g., Hansen et al., 2006; Al-Lazki et al., 2002). The thickness of the crust has been estimated as 33–37 km thick in northern Arabia and 41–53 km thick in the south (Al-Lazki et al., 2002). Mechie et al. (2013) imaged sharp changes in crustal thickness beneath the margins of the southern Red Sea and Gulf of Aden, probably due to the presence of high-velocity mafic bodies (Van Aven-donk et al., 2009). This was confirmed by the study of Ahmed et al. (2013), who imaged a transition from a 35-km-thick crust (inland) to a 14-km-thick crust (on the coast) across the Red Sea margin. Eastward in southern Oman the thickness of the crust was been estimated to vary from ~35 km inland to 26 km at the coast (Tiberi et al., 2007; Al-Hashmi et al., 2011).

Seismological studies have provided large-scale images of the lithosphere beneath the Arabian plate (e.g., Benoit et al., 2003; Park et al., 2007). In global surface-wave tomographic models, resolution is only achieved in the upper ~1000 km of the mantle. Chang and Van der Lee (2011) used tomography combined with gravity and receiver functions techniques to image the Arabian plate with a resolution of a few hundred kilometers. Hansen and Nyblade (2013) computed a P wave velocity model for eastern Africa and southern Arabia, with ~5° of resolution. These studies show that the central and eastern Gulf of Aden is characterized by normal wavespeed mantle.

Corbeau et al. (2014) studied the southern Arabian plate at a regional scale, using Pn tomography on a relatively dense collection of stations deployed in East Africa and Arabia, including our study region; their model displays low-velocity anomalies in the uppermost mantle lid under the recent volcanic zones in the Gulf of Aden. Corbeau et al. (2014) also suggested that transform faults may act as rheological barriers, thus diverting flow away from the ridge, toward present locations of recent volcanism. This would support the plume-ridge interaction model proposed in Leroy et al. (2010b), in which Afar plume material could be channeled beneath a narrow lithospheric corridor under the Aden ridge.



At a more local scale, the western Gulf of Aden was imaged in Korostelev et al. (2014) using teleseismic tomography, and inferred small-scale upwelling beneath young rift flank volcanoes. Basuyau et al. (2010) computed a P wave velocity model for the region of Dhofar (Oman) using the Dhofar Seismic Experiment network, and imaged two low-velocity anomalies in the upper mantle beneath the northern continuity of Alula-Fartak and Socotra-Hadbeen fracture zones; they also inferred partial melting associated with these two anomalies.

## ■ DATA

We significantly improve the understanding of mantle structure and melting processes beneath the eastern Gulf of Aden using data recorded by broadband seismic stations on the south of the Arabian plate. Data have been collected from 89 temporary broadband stations: 30 stations deployed during the 2003–2006 (Dhofar Seismic Experiment; used by Basuyau et al., 2010) and 59 stations deployed during March 2009 to March 2010 (YOCMAL project; Leroy et al., 2010a). The network extends from the city of Al Mukalla in Yemen to Ras Madrakah (58°E, 19°N) in the Sultanate of Oman (Fig. 2). The stations are all located <350 km from the sea, between the desert and the coast. They are not equally distributed in space because the area is not easily accessible. The impact of the stations distribution is discussed with the use of a checkerboard test. We selected 833 clear events of magnitude  $\geq 5.5$  (Fig. 3). Most of the events arrived as P (epicentral distance from 30° to 90°), and we also picked events that arrived as PP and PKP in order to improve azimuthal covering. The events were picked using SAC (Seismic Analysis Code; <http://ds.iris.edu/ds/nodes/dmc/forms/sac/>) software, after which we computed 11339 delay times with respect to the ak135 reference Earth model (Kennett et al., 1995). The 2003–2006 events were picked by Basuyau et al. (2010) using the waveform cross-correlation method of VanDecar and Crosson (1990). For the 2009–2011 events, we chose to hand-pick the earthquake arrivals as it took the same time and was more precise in our case. For each arrival, an error in arrival time was assigned (a, b, c, or d) within the range  $\pm 0.05$  to  $\pm 0.2$  s. Quality d (which equates to picking error of  $\pm 0.2$  s) was not used, and when no picking was possible due to noise, we discarded the data. We used a bandpass filter between 0.2 and 2 Hz.

## ■ METHOD

The key assumption of teleseismic tomography is that velocity variations located far from the network do not significantly affect relative arrival-time residuals derived from teleseismic body waves. We can thus determine velocity variations in the volume that is beneath the network of stations. The standard ACH method approach is to embed this local three-dimensional model volume within a global spherically symmetric reference model (Aki et al., 1977; Benz et al., 1992; Saltzer and Humphreys, 1997; Frederiksen et al., 1998). This allows rapid traveltime predictions to be made from the source to the boundary of

the local model. Then more sophisticated ray-tracing techniques are used to derive the heterogeneous local model.

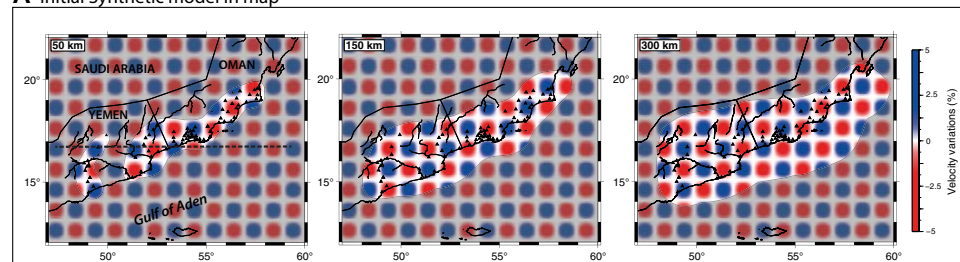
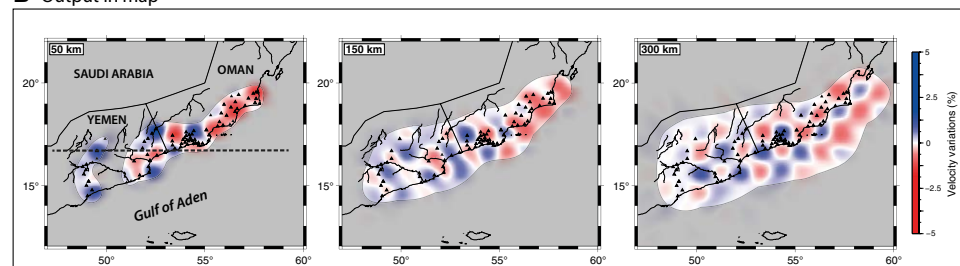
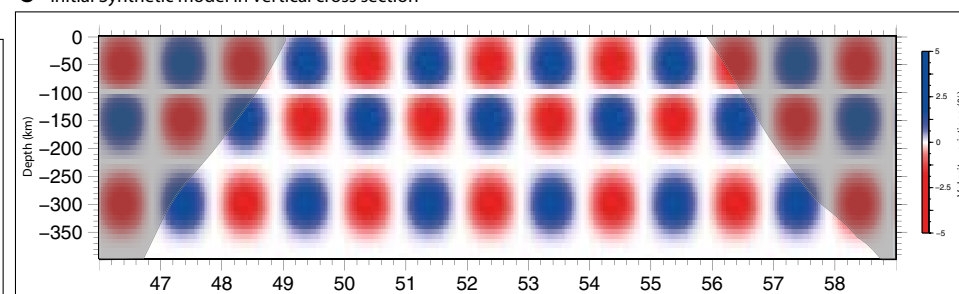
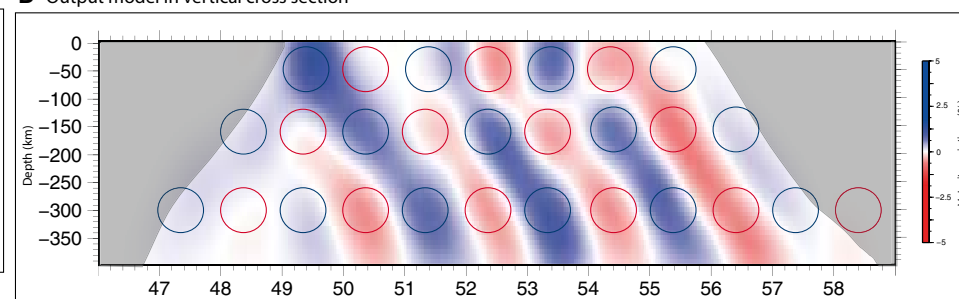
The iterative nonlinear method used in this study was developed by Rawlinson et al. (2006). The model is defined by a mesh of velocity nodes in spherical coordinates ( $0.25^\circ \times 0.25^\circ$ ). Traveltimes from each source to the base of the local model are computed through the ak135 global reference model using the approach of Kennett and Engdahl (1991). Then, the FMM method is used to compute traveltimes from the base of the local model to the network on the surface (e.g., Sethian, 1996, 1999, 2001; Sethian and Popovici, 1999; Rawlinson and Sambridge, 2005). The inversion is then computed using the subspace inversion method (Kennett et al., 1988).

For this study we selected a model composed of nine 50-km-thick layers, distributed from the surface down to 450 km. Horizontally, the node spacing is  $0.25^\circ \times 0.25^\circ$  (i.e., the average distance between two stations). The smoothing factor, which limits the short wavelength velocity variations, and the damping factor were chosen after a series of tradeoff tests following the approach of Rawlinson et al. (2006). Variations in damping and smoothing factors were tested in order to address the nonuniqueness of the solution. We chose a damping factor of 10 and smoothing factor of 5, which correspond to the values chosen by Rawlinson et al. (2006). The one-dimensional reference or starting model is ak135; 10 iterations are applied to the relative arrival-time residuals to produce a stable solution model. The solution model reduces the data variance by 76.5% from  $0.7998 \text{ s}^2$ – $0.01882 \text{ s}^2$ , which corresponds to a root mean square reduction from 282.8 ms to 137.2 ms. This data variance is also similar to 74% data variance achieved using the same method in Rawlinson et al. (2006). The remaining misfit can be attributed to factors such as crustal structures and mantle structure beneath the local model volume.

## Checkerboard Test

A synthetic checkerboard test is computed in order to investigate the robustness of the solution model. For this test we use the same sources, receivers, and phase types as in our data set to predict the arrival-time residuals for a synthetic checkerboard structure. To do that, we placed anomalies at 50, 150, and 300 km depth that alternate between slow and fast velocities (Figs. 4A, 4C). The anomalies are  $2 \times 2$  nodes in width. The data set calculated through this synthetic velocity model is then inverted, and the retrieved anomalies provide an indication of the resolution that can be achieved in our solution velocity model. Our network dimensions are ~350 km from north to south, and ~1100 km from west to east. According to Evans and Achauer (1993), our depth resolution corresponds to the lateral extent of our network at the surface. Thus, the maximum investigation depth of our teleseismic tomography study corresponds to the minimum lateral extent of our network, which is 350 km depth.

Figures 4B and 4D display the retrieved velocity models. At all depths, the resolution is best in the central part of our network, Dhofar (Oman), due to increased station density and crossing rays. The westernmost part of the net-

**A** Initial Synthetic model in map**B** Output in map**C** Initial Synthetic model in vertical cross section**D** Output model in vertical cross section

**Figure 4. Checkerboard test. (A)** Initial synthetic model in map. The dashed line indicates the location of the cross section. **(B)** Output model in map. **(C)** Initial synthetic model in cross section. **(D)** Output in cross section.

work consists of two profiles (in Yemen), so the distribution of the stations is linear and there are fewer ray crossings and poorer resolution. However, the synthetic checkerboard structures are distorted but can be retrieved. At depths of 150 and 300 km, the number of crossing rays increases under the region, so the resolution improves. Under 400 km, the rays are too dispersed to reliably interpret the structures.

## RESULTS

### Structures at Shallow Depth

The result of our inversion displays anomalies with a higher amplitude (ranging  $-3.75\%$  to  $+5\%$ ) at crustal depth ( $\leq 30$  km) in the west of the study area (Fig. 5). From Hasik ( $56^\circ\text{E}$ ,  $18^\circ\text{N}$ ) to the Ras Madrasah peninsula ( $58^\circ\text{E}$ ,  $19^\circ\text{N}$ , Fig. 2), velocity anomalies are low amplitude. The anomalies imaged at crustal depth can be related to geological structures observed at the surface. Generally, low-velocity anomalies are at sedimentary basins, and high-velocity anomalies are beneath basement outcrops. The crustal low-velocity anomalies located

along the coast of eastern Yemen could be related to the Masilah and Jiza-Qamar basins, filled with Jurassic (for Masilah) or Campanian (for Jiza-Qamar) to Paleocene–early Eocene sediments (Fig. 6A). However, these low-velocity anomalies are also located near volcanic fields, such as Al-Mukalla or Wadi Masilah (purple shaded areas, Fig. 2). This may suggest that low velocities are caused by partial melt and elevated temperatures within the plumbing systems associated with these volcanoes. A positive velocity anomaly in the eastern part of Yemen near Thamud ( $50^\circ\text{E}$ ,  $17.5^\circ\text{N}$ ) is associated with the Cretaceous Hadramaut arch (Fig. 2), and one east of Salalah ( $54^\circ\text{E}$ ,  $17^\circ\text{N}$ ) is consistent with Mirbat Precambrian basement outcrop along the margin, where prerift sedimentary cover is absent. In southern Oman, two other low-velocity anomalies may correspond to the Ashawq basin depocenter and to the 3 km of sediments deposited in the Salalah plain (Fig. 6A). The low-velocity anomalies of southern Dhofar are close to the Ashawq-Salalah volcanic zone mapped by bathymetry and seismic data in the Ashawq-Salalah segment (Autin et al., 2010; Lucazeau et al., 2008; Leroy et al., 2010b) (Fig. 2, purple shaded area). Near Ras Madrasah ( $58^\circ\text{E}$ ,  $19^\circ\text{N}$ ) the low-velocity anomaly in the easternmost part of our study area seems to be consistent with a Cretaceous sedimentary basin partly covered by the Masirah ophiolite (Robinet, 2013; Robinet et al., 2013).

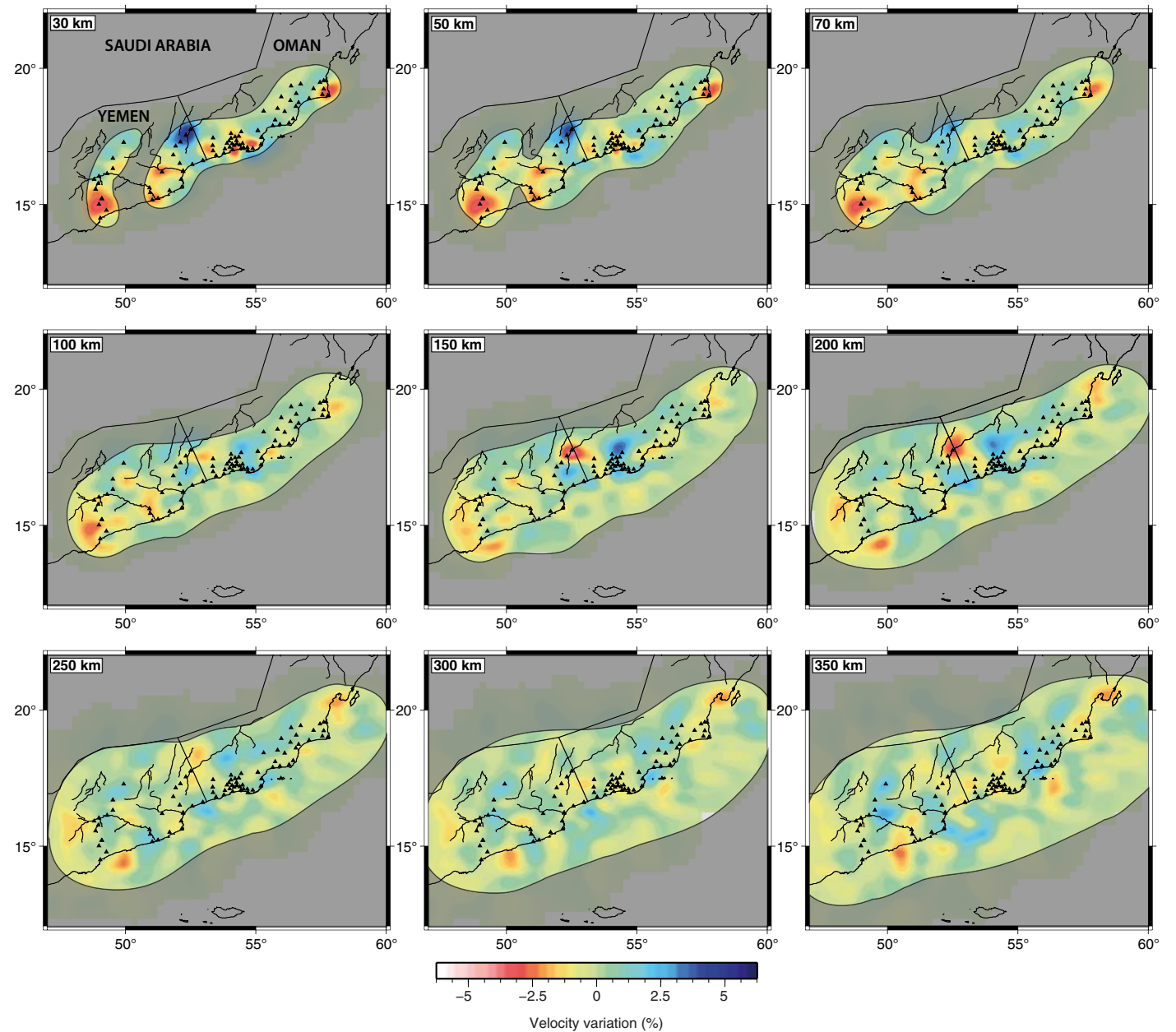


**Figure 5.** Final P wave velocity model obtained from inversion at depth from 30 to 350 km. Seismic stations are located by black triangles. The black lines delimit the best constrained tomographic model.



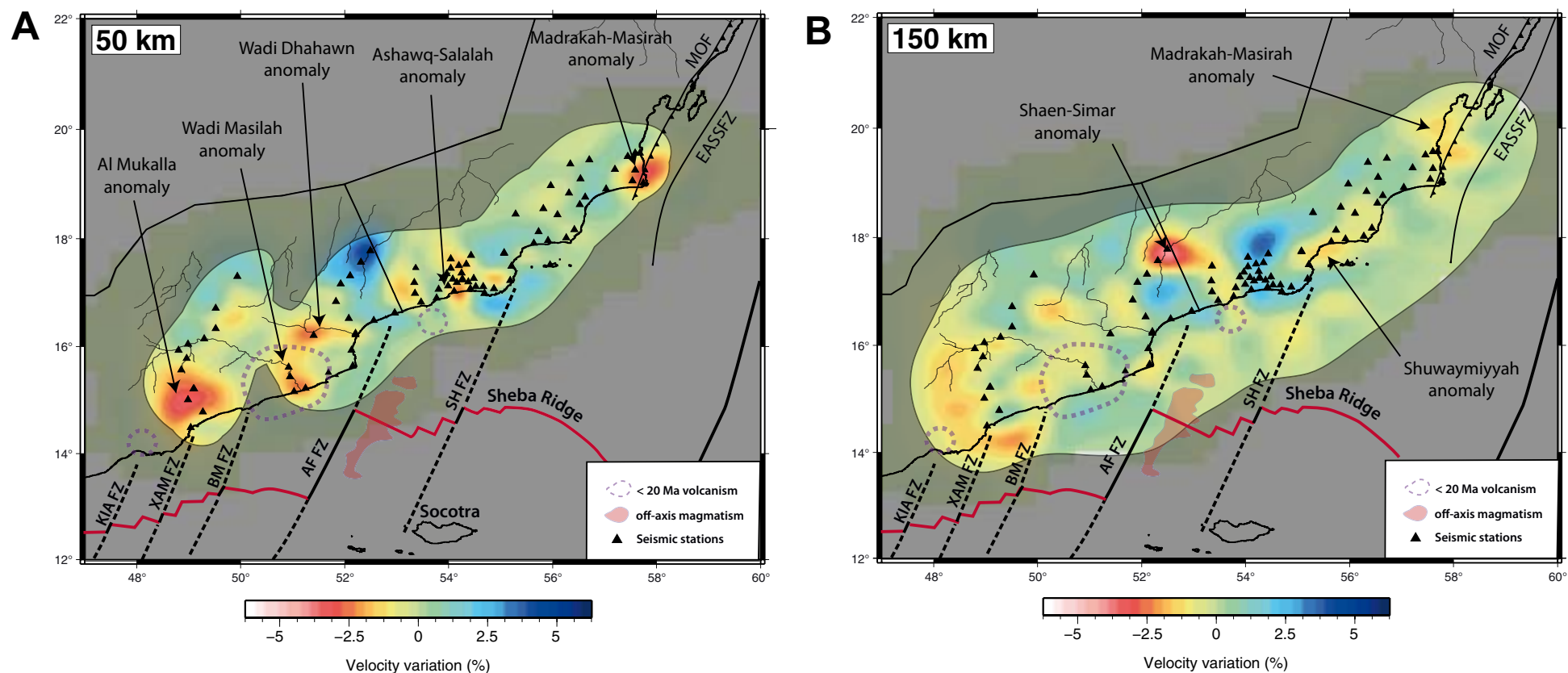


Figure 6. Horizontal cross sections in the final P wave velocity model obtained from inversion. (A) 50 km depth. (B) 150 km depth. KAIFZ—Khanshir Al Irqah fracture zone; XAMFZ—Xiis–Al Mukalla fracture zone; BMFZ—Bosaso–Masilah fracture zone; AFFZ—Alula–Fartak fracture zone; SHFZ—Socotra–Hadbeen fracture zone; EASSFZ—East Arabian strike-slip fault zone; MOF—Masirah ophiolite front. The solid gray line delimits the best constrained model.

### Structures Observed at Depth

The mantle beneath central and eastern Yemen is not homogeneous, but is characterized by variations in seismic velocity. Generally, low-velocity anomalies are observed in discrete lobes that are 100–300 km in width. The Al Mukalla low-velocity anomaly (Fig. 6A) is located at the northward continuity of Xiis–Al Mukalla fracture zone, and west of Bosaso–Masilah fracture zone. This anomaly can be observed from the surface to the bottom of our velocity model (Fig. 7, cross-sections A–A' and B–B'; Fig. 8, cross-section F–F'), with a maximum amplitude at 50 km depth. The anomaly is close to Al Mukalla volcano (Fig. 6; Fig. 7, cross-section A–A'; Fig. 8, cross-section F–F').

Under the Wadi Masilah and Wadi Dhahawn zones, there are low-velocity anomalies that join at ~100 km depth (Fig. 7, cross-section B–B'; Fig. 8, cross-section G–G'). As we have no resolution between Al Mukalla, Wadi Masilah, and Wadi Dhahawn for the upper 100 km, we cannot determine if these anomalies are one linked feature or multiple low-velocity anomalies. Their maximum amplitude is ~2.5% for Wadi Masilah and Wadi Dhahawn and ~3.75% for Al Mukalla at 50 km depth. Deeper, the amplitude decreases, but low velocities are still present to depths of 350 km.

The Shaen-Simar (52.5°E, 17.5°N) low-velocity anomaly was imaged by Basuyau et al. (2010) as between 60 and 200 km depth, with a width of ~100 km. We retrieve this anomaly at the same location and same depth range, as seen in Figures 5 and 7 (cross-section C–C'). The Shuwaymiyyah

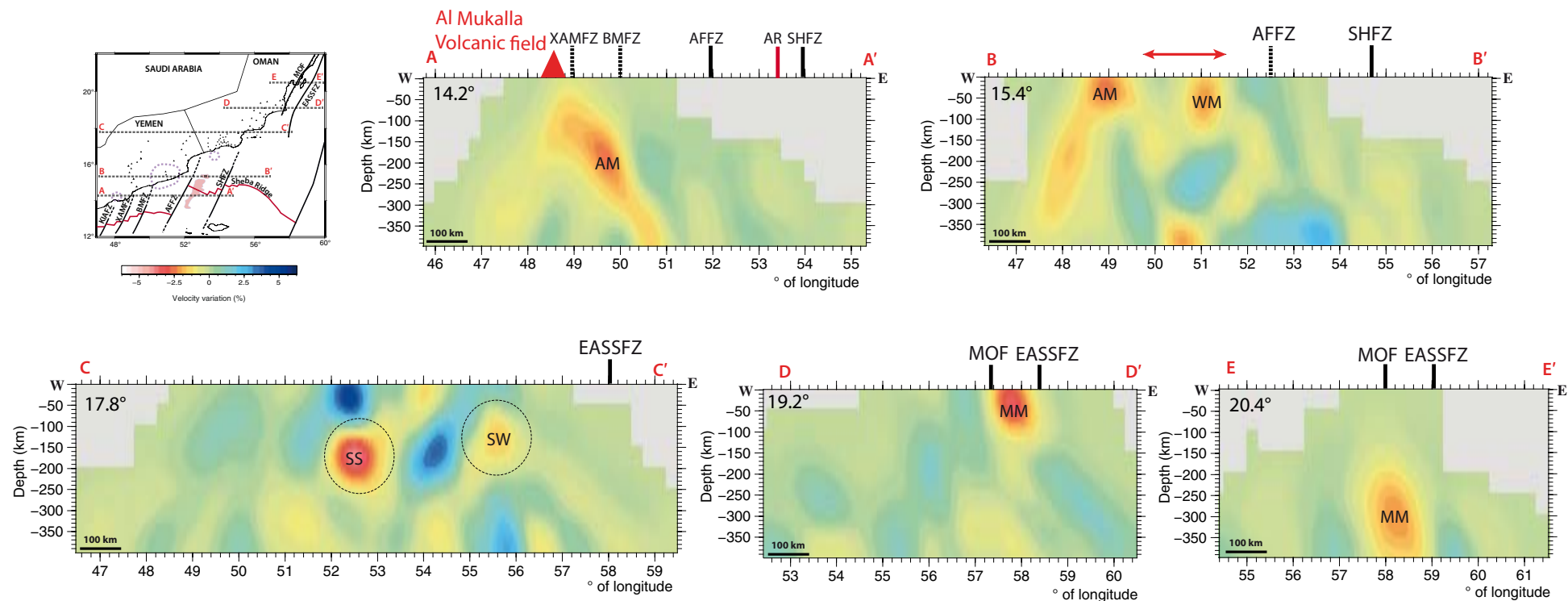


Figure 7. Latitudinal cross sections in the solution P wave velocity model obtained from inversion. Dashed circles on the cross sections correspond to low-velocity anomalies imaged in Basuyau et al. (2010). The latitude is on the top left of each cross section. KAIFZ—Khanshir Al Irqah fracture zone; XAMFZ—Xiis-Al Mukalla fracture zone; BMFZ—Bosaso-Masilah fracture zone; AFFZ—Al-ula-Fartak fracture zone; SHFZ—Socotra-Hadbeen fracture zone; EASSFZ—East Arabian strike-slip fault zone; MOF—Masirah ophiolite front; AR—Aden ridge; AM—Al Mukalla anomaly; MM—Madrakah-Masirah anomaly; SS—Shaen-Simar anomaly; SW—Shuwaymiyyah anomaly; WM—Wadi Masilah anomaly.

low-velocity anomaly (55.5°E, 17.5°N, Fig. 5; Fig. 7, cross-section C-C'; Fig. 8, cross-section I-I') corresponds to their eastern anomaly. We also retrieve it at the same location and depth range. This anomaly seems to be smaller than that at Shaen-Simar (52.5°E, 17.5°N), and to have a lower amplitude (~1.8% at 100 km depth). These two anomalies are imaged along the landward continuation of two main fracture zones, Alula-Fartak and Socotra-Hadbeen. Owing to a greater number of stations, and a wider spatial extent of the network, we achieve better resolution for these two anomalies; they were on the edges of the model of Basuyau et al. (2010), and are now at the center of our network, so they are better constrained.

The last important low-velocity anomaly displayed in our model (Madrakah-Masirah, Fig. 5; Fig. 7, cross-sections D-D', E-E'; Fig. 8, cross-section G-G') is located in the extreme part of the Ras Madrakah (58°E, 19°N) peninsula at 0–70 km depth, and then it deepens toward the north-northeast (to 58.25°E,

20°N). As the network did not extend to Masirah Island (58.5°E, 20.5°N), our model only places some constraints on structure below 200 km near the southern edge of our study region (Fig. 7, cross-section E-E'; Fig. 8, cross-section J-J'). This anomaly is located between the Masirah ophiolite front and the East Arabian strike-slip fault zone (Figs. 6A, 6B).

## DISCUSSION

Our study provides an image of the structure of the lithosphere and upper asthenosphere below the southern Arabia passive continental margin. These results allow us to discuss the influence of major transform faults on the passive continental margins and the origin of surface structures of the margin, such as volcanoes and topography.

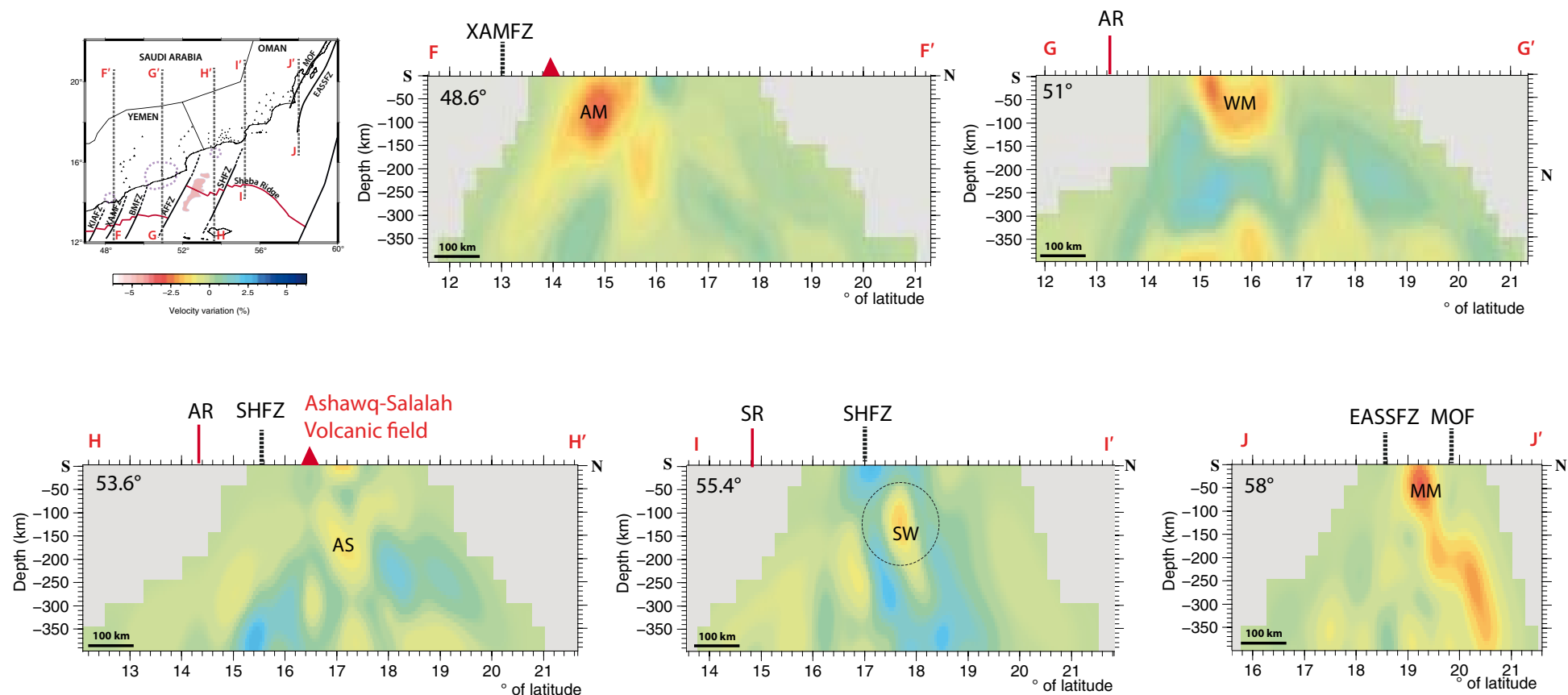


Figure 8. Longitudinal cross sections in the solution P wave velocity model obtained from inversion. Dashed circles on the cross sections correspond to low-velocity anomalies imaged in Basuyau et al. (2010). The longitude is on the top left of each cross section. KAIFZ—Khanshir Al Irqah fracture zone; XAMFZ—Xiis-Al Mukalla fracture zone; BMFZ—Bosaso-Masilah fracture zone; AFFZ—Alula-Fartak fracture zone; SHFZ—Socotra-Hadbeen fracture zone; EASSFZ—East Arabian strike-slip fault zone; MOF—Masirah ophiolite front; AR—Aden ridge; SR—Sheba ridge; AM—Al Mukalla anomaly; AS—Ashawq-Salalah anomaly; MM—Madrakah-Masirah anomaly; SW—Shuwaymiyyah anomaly; WM—Wadi Masilah anomaly.

### Transform Fault Zones and Volcanism

The low velocities observed in our model are located beneath the passive continental margin of the Gulf of Aden, in the vicinity of major fracture zones. Models predict that the thermal anomaly created by synrift mantle upwelling will cool after breakup. For the Gulf of Aden, models of post-breakup thermal relaxation predict that the mantle cooled by 50 °C since breakup ca. 18 Ma (Lucazeau et al., 2008). The low-velocity anomalies are therefore unlikely due to the synrift thermal or melt related anomalies, since they should have cooled. An alternative mechanism is required.

King and Anderson (1998) inferred that at the edge of a continent, the thermal conditions drive a strong and unsteady flow. This means that the conditions of the lithosphere can promote mantle flow at the edges of continents. Numerical modeling by Morency et al. (2005) computed that ~30–40 m.y. after rifting, downward instabilities and then small-scale convection can develop under a cooling oceanic lithosphere. This is likely to occur near the ocean-continent transition (Lucazeau et al., 2008, 2009, 2010). Moreover, in the case of transform faults, instabilities develop for each fault, much faster (~16 m.y.) than under an oceanic lithosphere without transform faults. Transform faults juxtapose lithosphere of different ages and thicknesses (e.g., Dumoulin et al., 2008).



Flow initiates under the lithosphere from the young side toward the old side of the transform fault, with thermal erosion of the thick lithosphere (Fig. 9; Dumoulin et al., 2008; Gerya, 2013). The lithospheric steps at depth and the location of the fracture zones at the surface show an offset; consequently, volcanoes can be observed on the old side of the fracture zone. Sleep (2002) noticed this paradox of volcanoes located on the old side of fracture zones, and explained it by additional heat supplied by small-scale convection under the lithosphere and by disappearance of lithospheric relief beneath a fracture zone. The magmatism may have no expression at the surface (Fig. 9).

Our study area is located at the edge of a continent, and is segmented by major fracture zones. The natural conditions are therefore similar to those in the model of Dumoulin et al. (2008). The oceanic lithosphere is older than 16 Ma, and so small-scale convection can initiate in the vicinity of fracture zones (Morency et al., 2005). In our model, we image several low-velocity anomalies along the Gulf of Aden, from the surface to our maximum investigation depth (Fig. 5). Basuyau et al. (2010) noted two low-velocity anomalies in Dhofar from 60 to 200 km depth in the continuation of the Alula-Fartak and Socotra-Hadbeen fracture zones (Fig. 5). Channelization of a mantle flow from the Afar hotspot along the oceanic ridge and the fracture zones is invoked to explain these anomalies as well as the numerous active volcanoes (Leroy et al., 2010b; Corbeau et al., 2014).

The other low-velocity anomalies of our velocity model are also close to fracture zones (between 0 and 100 km), the Xiis–Al Mukalla and Bosaso–

Masilah fracture zones, and the East Arabian strike-slip fault. Their locations could also be consistent with a small-scale convection model (Fig. 6A).

## Dynamic Topography and Uplift of the Southern Arabian Plate

The Gulf of Aden continental northern margin is characterized by elevated plateaus of more than 1000 m high, incised by a network of wadis (seasonal rivers). These high plateaus are located between the sea and Rub' Al Khali desert (Fig. 10). Higher plateaus are found to the west of our study zone (Hadramaut plateaus, ~1000 m high), and lower ones are found to the east.

A residual topography model was computed by Daradich et al. (2003) by correcting the observed topography for crustal thickness variations assuming isostatic compensation of the crust. This residual topography map shows two zones of high topography dynamically supported by upper mantle structures in the eastern Gulf of Aden. The first extends from Al Mukalla to the Jiza-Qamar basin, and the second is north of Mirbat (57°E, 17.5°N, Fig. 2). Daradich et al. (2003) explained that elevated topography is dynamically supported by seismically slow and thermally buoyant structures in the upper mantle.

In order to investigate whether the elevated topography observed in our study region is only due to isostatic compensation or could be supported dynamically (i.e., by hot mantle indicated by the low-velocity anomalies of our

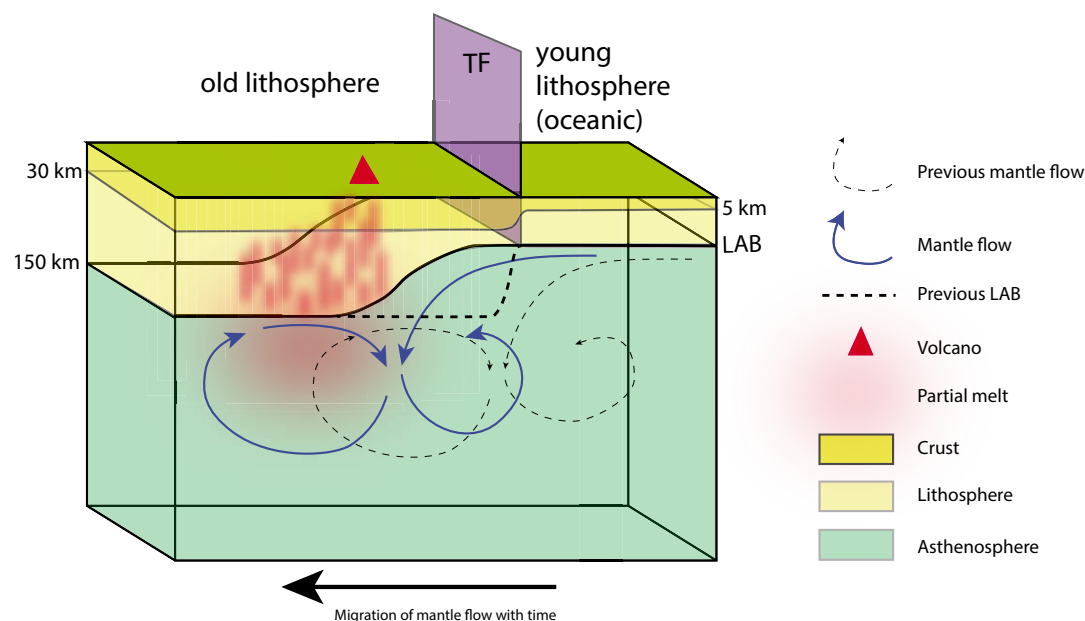


**Figure 9.** Conceptual sketch of the small-scale convection initiating beneath a step in the lithosphere-asthenosphere boundary (LAB) topography due to a transform fault (TF; based on the models of Dumoulin et al., 2008). As the edge of the lithosphere is eroded, the mantle flow migrates toward the thicker (old) side of the transform fault over time.

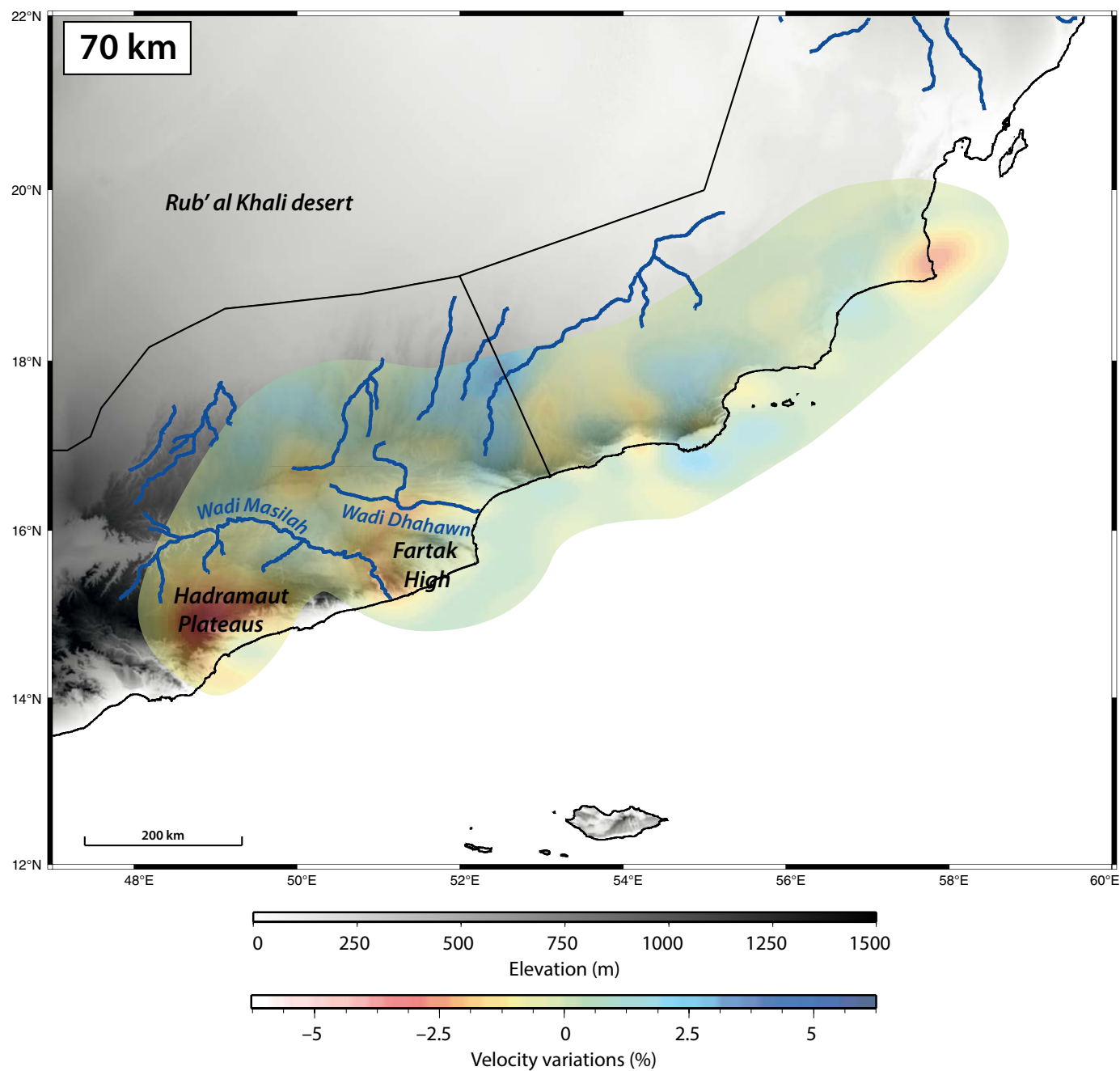


Figure 10. Map of the eastern Gulf of Aden margin displaying the topography, rivers, and a cross section of our solution model at 70 km depth. The bathymetry is not displayed.

model), we determined the expected elevation of the central and eastern Gulf of Aden margins using lithospheric isostatic balancing. We use the crustal thickness estimated by receiver functions in Yemen (our data) and Dhofar (Tiberi et al., 2007; Leroy et al., 2012; this study) and a 100-km-thick lithosphere to calculate the isostatic topography  $z_{iso}$  (Fig. 11):

$$z_{iso} = (f_1 l_c + f_2 l_m) - H, \quad (1)$$

where  $l_c$  is the crust thickness,  $l_m$  is the lithosphere thickness,  $f_1 = (\rho_a - \rho_c)/\rho_a$ , and  $f_2 = (\rho_a - \rho_m)/\rho_a$ . Estimating that the isostatic topography matches the observed topography for a 40-km-thick crust (density  $\rho_c = 2850 \text{ kg/m}^3$ ) and a 100-km-thick lithosphere (density  $\rho_m = 3250 \text{ kg/m}^3$ ) requires an asthenosphere density ( $\rho_a$ ) of  $3180 \text{ kg/m}^3$ . The average mid-oceanic ridge elevation,  $H$ , is 2.4 km (Lachenbruch and Morgan, 1990). The residual topography is derived from the difference between the observed and isostatic topography.

These rapid computations only allow us to interpret general trends rather than short wavelength variations; there can be errors of a few kilometers on

the crustal thickness estimated by receiver functions. In Yemen and in Dhofar, the margin is not at isostatic equilibrium (i.e., the observed and isostatic topography do not match; see Fig. 11). The observed topography is higher than the isostatic topography, so we have a positive residual topography. This means that the observed topography cannot be explained by isostasy. Therefore, there is probably dynamic support for the topography in the region from the presence of buoyant upper mantle. This support seems weaker in the eastern part of the model, as the topographies are much lower than in the west. It is also possible that the denudation of the margin plays an important role in its uplift, as isostatic response to erosion is often a large component of surface uplift rate (Molnar and England, 1990).

The structures imaged by Daradich et al. (2003) coincide with the low-velocity zones imaged in our solution model at upper mantle depths of 50 and 70 km depth. Their resolution is only  $\sim 1 \text{ pixel}/100 \text{ km}$ . With our velocity model, however, we can decipher several smaller low-velocity zones. In Figure 10 we can see an image of the upper mantle velocity anomalies (at 70 km depth) on a topographic map. The largest wadi in Yemen, Wadi Masilah ( $51^\circ\text{E}$ ,

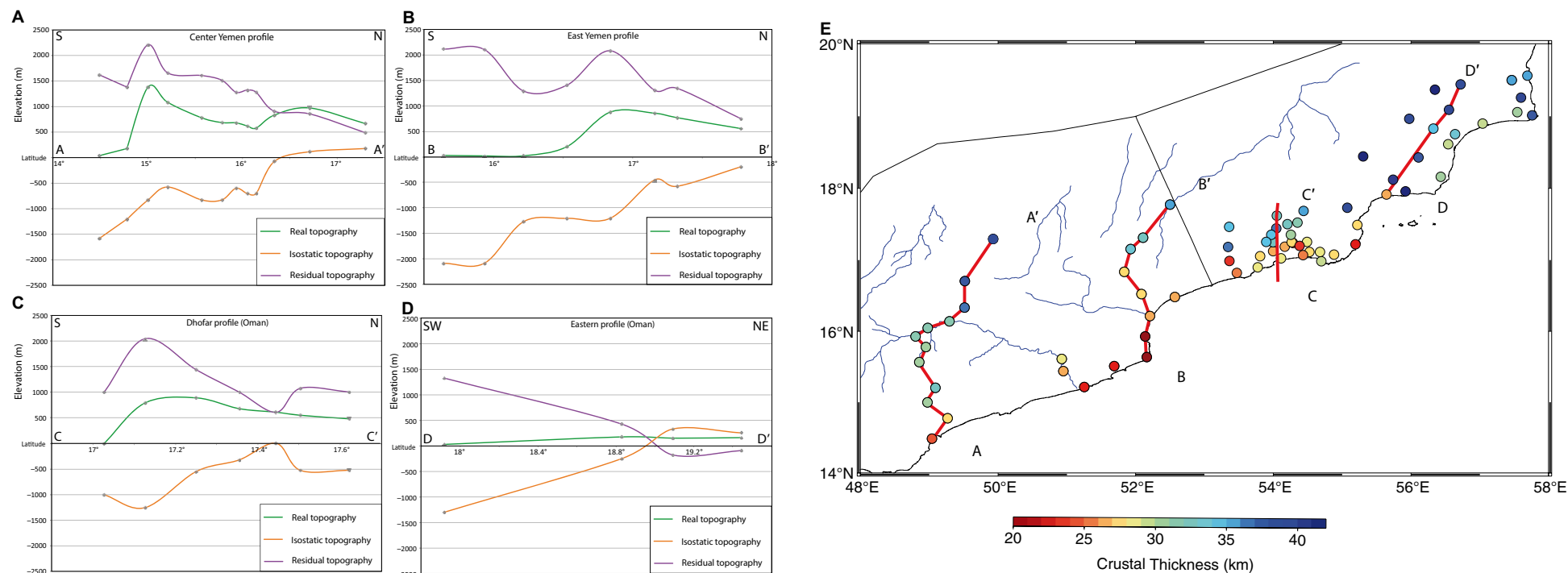


**Figure 11.** Observed, isostatic, and residual topography for four profiles in the central and eastern Gulf of Aden margin. These rapid computations only allow us to interpret general trends and not short wavelengths, as there can be errors of a few kilometers on the crustal thickness estimated by receiver functions. (A) Profile across central Yemen. (B) Profile across eastern Yemen. (C) Profile across Dhofar (Oman). (D) Profile parallel to the margin in southeastern Oman. (E) Crustal thickness and locations of the profiles.



15°N), crosses the Hadramaut region and is bounded by low-velocity anomalies to the south and north. The northern anomaly corresponds to high topography and is the starting point for another wadi, heading toward Rub' Al Khali desert (Saudi Arabia). The southern low-velocity anomaly is located under the Hadramaut plateaus. Between Wadi Masilah and Wadi Dhahawn, under the Fartak high (52°E, 15.5°N), another low velocity can be observed. In the Ras Madrasah peninsula (58°E, 19°N), the strong low-velocity anomaly in the upper mantle corresponds to a localized area elevated to 150 m with respect to the surroundings.

Several models have been developed in order to explain why uplift can occur. In thermal models, Keen (1985) and Buck (1986) proposed that uplift can result from heating of the rift flanks by small-scale convection during rifting. For others (e.g., Cox, 1980; White and McKenzie, 1989), uplift could result from magmatic underplating due to the partial melting of the asthenosphere. However, even if the sea level was never high in central Yemen (lacustrine sedimentation; Leroy et al., 2012), the uplift observed in the central and eastern Gulf of Aden is recent and postrift (e.g., Bunce et al., 1974; Beydoun, 1991; Autin et al., 2010), and no large magmatic underplating has been described previously.

Traveltime tomography gives the present state of the upper mantle in terms of velocity variations, but it precludes any direct interpretation concerning their origin. Several factors, such as temperature, chemical composition, or anisotropy, can affect the velocity of seismic waves (e.g., Karato, 1993; Sobolev et al., 1996). Low-velocity anomalies are generally interpreted as of thermal origin in the mantle. The abnormally slow features observed in our solution model could correspond to abnormally hot and buoyant upper mantle structures. Uplift can then be created by buoyancy due to elevated mantle temperatures. The links between mantle structures and uplift have been studied at the large scale (e.g., Burke, 1996; Gurnis et al., 2000; Daradich et al., 2003). It is commonly accepted that large mantle structures such as a mantle plume can cause topographic swells of as much as 2 km in elevation and many hundreds to a few thousands of kilometers in diameter (e.g., Şengör, 2001; Saunders et al., 2007; Gurnis et al., 2000; Forte et al., 2010; Faccenna et al., 2014).

The elastic-viscous-plastic model of Burov and Guillou-Frottier (2005) predicts that upper mantle structure can produce transient topographic signatures such as uplift and subsidence at a large (>500 km) and small scale (down to 50–100 km). For an upper mantle structure of diameter 100 km, located between 100 and 200 km depth, the range of wavelength for an observable topographic signature will be 50–100 km (Burov and Guillou-Frottier, 2005). Therefore, the low-velocity–high-temperature structures that we observe in our solution model may trigger small-scale uplift on the Gulf of Aden northern margin.

The anomalously hot and buoyant upper mantle structures imaged in our model could have uplifted the central and eastern Gulf of Aden margin. At a smaller scale, these processes could have uplifted the Fartak high and thus have shifted the bed of Wadi Masilah, creating another smaller river, Wadi Dhahawn. This is consistent with the analysis of Bunce et al. (1974), in which they presented evidence for a shift of drainage area from Wadi Dhahawn

to the southern Wadi Masilah; they noticed a large volume of sediments in Deep Sea Drilling Project Site 232 (Leg 24), to the west of Alula-Fartak fracture zone, just in the continuity of Wadi Masilah. In these sediments, several slumping episodes dated 6–5 Ma mark one or more tectonic events related to the uplift of the margin (Bunce et al., 1974). Moreover, the bathymetric and seismic reflection study of Baurion (2009) confirmed that the large volume of sediments offshore Wadi Dhahawn are not consistent with the present-day drainage area. According to Baurion, 2009, the Fartak high was uplifted ca. 10 Ma and cut Wadi Masilah into two smaller wadis. As a consequence the upper mantle small-scale convection can have an important effect on the drainage network through generation of topography. This has been shown at a large scale in Africa (Moucha and Forte, 2011). In addition in Oman, Roger et al. (1989), Platel and Roger (1989), and Leroy et al. (2012) explained the presence of Dhofar paleobeaches (beach rock) 13–25 m above sea level by a very recent rapid uplift of the region (post-2 Ma to present). These elevated features are above low velocities in our model (Ashawq and north of the city of Salalah).

## CONCLUSIONS

We used teleseismic relative arrival-time tomography to compute a P wave velocity model of the upper mantle beneath the central and eastern Gulf of Aden margins. The strong correlation between low velocities in the mantle and region of uplift strongly suggests that mantle processes create dynamic support of the topography of the Hadramaut plateaus (Yemen to 56°E, 18°N, and Oman), and for the easternmost part of the Ras Madrasah peninsula (58°E, 19°N, Oman). The plateaus created by the uplift likely affect the course of wadis and the sedimentation at the mouth of the wadis. The localized nature of the low-velocity structures and spatial correlation to volcanism at the surface suggests that they are the expression of small-scale convection created by the step in temperatures and thickness of lithosphere at the edge of the Arabian plate. The transform faults create another step between two distinct types of lithosphere (old versus young) and can also trigger small-scale convection. Our work shows that spatially localized postrift magmatism in predominantly magma-poor rifted margins can be caused by localized small-scale convection focused near the steps in lithosphere–asthenosphere boundary topography and mantle temperatures at the juncture between fracture zones and the rifted margin. Such a mechanism facilitates both volcanism and localized dynamic uplift of the rifted margin well after breakup has occurred.

## ACKNOWLEDGMENTS

This project was funded by the ANR (Agence Nationale de la Recherche) project YOCMAL 07-BLAN-0135, CNRS-INSU-PICS (Centre National de la Recherche Scientifique–Institut National des Sciences de l'Univers–International Programs for Scientific Cooperation) Yemen and Oman, and the Geological Survey and Mineral Resources Board (GSMRB, Yemen), and is in the frame-

work of the Actions Marges program. Seismic equipment from SEIS-UK is funded by the Natural Environment Research Council (NERC) under agreement R8/H10164. We thank David Hawthorn, Alex Brisbane, Victoria Lane, Christel Tiberi, Elia d'Acremont, Francis Lucazeau, François Bache, Jeffrey Poort, Céline Baurion, Jordane Corbeau, Ali Al-Lazki, and Khalfan Al-Toubi for their efforts during the deployment and servicing of the network, the French Embassy in Yemen (J.G. Sarkis, J. Dechezlepretre, and C. Bousquet), local governors, the people of the Yemen governorates and Directorate General of Minerals in Muscat and Salalah, Ali Al-Rajhi from Geological Survey and Sultan Qaboos University for their help during the field work. We also thank Martin Mai, an anonymous reviewer, and Associate Editor Carolina Pagli. Keir is supported by NERC grant NE/L013932/1.

## REFERENCES CITED

- Ahmed, A., Tiberi, C., Leroy, S., Stuart, G.W., Keir, D., Sholan, J., Khanbari, K., Al-Ganad, I., and Basuyau, C., 2013, Crustal structure of the rifted volcanic margins and uplifted plateau of western Yemen from receiver function analysis: *Geophysical Journal International*, v. 193, p. 1673–1690, doi:10.1093/gji/ggt072.
- Aki, K., Christoffersson, A., Husebye, E., and Powell, C., 1974, Three-dimensional seismic velocity anomalies in the crust and upper-mantle under the USGS, California seismic array: *Eos (Transactions, American Geophysical Union)*, v. 56, p. 1145.
- Aki, K., Christoffersson, A., and Husebye, E., 1977, Determination of the three-dimensional seismic structure of the lithosphere: *Journal of Geophysical Research*, v. 82, p. 277–296, doi:10.1029/JB082i002p00277.
- Al-Hashmi, S., Gök, R., Al-Toubi, K., Al-Shijbi, Y., El-Hussain, I., and Rodgers, A., 2011, Seismic velocity structure at the southeastern margin of the Arabian Peninsula: *Geophysical Journal International*, v. 186, p. 782–792, doi:10.1111/j.1365-246X.2011.05067.x.
- Al-Lazki, A., Seber, D., Sandvol, E., and Barazangi, M., 2002, A crustal transect across the Oman Mountains on the eastern margin of Arabia: *GeoArabia*, v. 7, p. 47–78.
- Armitage, J., Collier, J., and Minshull, T., 2010, The importance of rift history for volcanic margin formation: *Nature*, v. 465, no. 7300, p. 913–917, doi:10.1038/nature09063.
- Autin, J., Leroy, S., Beslier, M., d'Acremont, E., Razin, P., Ribodetti, A., Bellahsen, N., Robin, C., and Al Toubi, K., 2010, Continental break-up history of a deep magma-poor margin based on seismic reflection data (northeastern Gulf of Aden margin, offshore Oman): *Geophysical Journal International*, v. 180, p. 501–519, doi:10.1111/j.1365-246X.2009.04424.x.
- Bastow, I.D., and Keir, D., 2011, The protracted development of the continent-ocean transition in Afar: *Nature Geoscience*, v. 4, p. 248–250, doi:10.1038/ngeo1095.
- Bastow, I., Nyblade, A., Stuart, G., Rooney, T., and Benoit, M., 2008, Upper mantle seismic structure beneath the Ethiopian hot spot: Rifting at the edge of the African low-velocity anomaly: *Geochemistry, Geophysics, Geosystems*, v. 9, no. 12, Q12022, doi:10.1029/2008GC002107.
- Basuyau, C., Tiberi, C., Leroy, S., Stuart, G., Al-Lazki, A., Al-Toubi, K., and Ebinger, C., 2010, Evidence of partial melting beneath a continental margin: Case of Dhofar, in the northeast Gulf of Aden (Sultanate of Oman): *Geophysical Journal International*, v. 180, p. 520–534, doi:10.1111/j.1365-246X.2009.04438.x.
- Baurion, C., 2009, Processus d'initiation et d'évolution des instabilités et canyons sous-marins de la marge nord du golfe d'Aden [M.S. thesis]: Institut des Sciences de la Terre de Paris, Université Pierre et Marie Curie (Paris 6), 53 p.
- Bellahsen, N., Husson, L., Autin, J., Leroy, S., and d'Acremont, E., 2013, The effect of thermal weakening and buoyancy forces on rift localization: Field evidences from the Gulf of Aden oblique rifting: *Tectonophysics*, v. 607, p. 80–97.
- Benoit, M., Nyblade, A., VanDecar, J., and Gurrrola, H., 2003, Upper mantle P wave velocity structure and transition zone thickness beneath the Arabian Shield: *Geophysical Research Letters*, v. 30, 1531, doi:10.1029/2002GL016436.
- Benz, H., Zandt, G., and Oppenheimer, D., 1992, Lithospheric structure of northern California from teleseismic images of the upper mantle: *Journal of Geophysical Research*, v. 97, p. 4791–4807, doi:10.1029/92JB00067.
- Beydoun, Z.R., 1991, Arabian plate hydrocarbon geology and potential—A plate tectonic approach: *American Association Petroleum Geologists Studies in Geology* 33, 77 p.
- Bown, J.W., and White, R.S., 1995, Effect of finite extension rate on melt generation at rifted continental margins: *Journal of Geophysical Research*, v. 100, p. 18,011–18,029, doi:10.1029/94JB01478.
- Buck, W.R., 1986, Small-scale convection induced by passive rifting: The cause for uplift of rift shoulders: *Earth and Planetary Science Letters*, v. 77, p. 362–372, doi:10.1016/0012-821X(86)90146-9.
- Bunce, E.T., et al., 1974, Site 232, in Fisher, R.L., et al., eds., Initial reports of the Deep Sea Drilling Project, Volume 24: Washington, D.C., U.S. Government Printing Office, p. 127–196, doi:10.2973/dsdp.proc.24.103.1974.
- Burke, K., 1996, The African plate: *South African Journal of Geology*, v. 99, p. 341–409.
- Burov, E., and Guillou-Frotier, L., 2005, The plume head–continental lithosphere interaction using a tectonically realistic formulation for the lithosphere: *Geophysical Journal International*, v. 161, p. 469–490, doi:10.1111/j.1365-246X.2005.02588.x.
- Chang, S., and Van der Lee, S., 2011, Mantle plumes and associated flow beneath Arabia and East Africa: *Earth and Planetary Science Letters*, v. 302, p. 448–454, doi:10.1016/j.epsl.2010.12.050.
- Chang, S., Merino, M., Van der Lee, S., Stein, S., and Stein, C., 2011, Mantle flow beneath Arabia offset from the opening Red Sea: *Geophysical Research Letters*, v. 38, L04301, doi:10.1029/2010GL045852.
- Corbeau, J., Rolandone, F., Leroy, S., Al-Lazki, A., Keir, D., Stuart, G., and Stork, A., 2014, Uppermost mantle velocity from Pn tomography in the Gulf of Aden: *Geosphere*, v. 10, p. 958–968, doi:10.1130/GES01052.1.
- Cox, K., 1980, A model for flood basalt volcanism: *Journal of Petrology*, v. 21, p. 629–650, doi:10.1093/petrology/21.4.629.
- d'Acremont, E., Leroy, S., Beslier, M., Bellahsen, N., Fournier, M., Robin, C., Maia, M., and Gente, P., 2005, Structure and evolution of the eastern Gulf of Aden conjugate margins from seismic reflection data: *Geophysical Journal International*, v. 160, p. 869–890, doi:10.1111/j.1365-246X.2005.02524.x.
- d'Acremont, E., Leroy, S., Maia, M., Patriat, P., Beslier, M.-O., Bellahsen, N., Fournier, M., and Gente, P., 2006, Structure and evolution of the eastern Gulf of Aden: Insights from magnetic and gravity data (Encens-Sheba MD117 cruise): *Geophysical Journal International*, v. 165, p. 786–803, doi:10.1111/j.1365-246X.2006.02950.x.
- d'Acremont, E., Leroy, S., Maia, M., Gente, P., and Autin, J., 2010, Volcanism, jump and propagation on the Sheba ridge, eastern Gulf of Aden: Segmentation evolution and implications for oceanic accretion processes: *Geophysical Journal International*, v. 180, p. 535–551, doi:10.1111/j.1365-246X.2009.04448.x.
- Daradich, A., Mitrovica, J., Pysklywec, R., Willett, S., and Forte, A., 2003, Mantle flow, dynamic topography, and rift-flank uplift of Arabia: *Geology*, v. 31, p. 901–904, doi:10.1130/G19661.1.
- Debaille, E., Lévêque, J., and Cara, M., 2001, Seismic evidence for a deeply rooted low-velocity anomaly in the upper mantle beneath the northeastern Afro-Arabian continent: *Earth and Planetary Science Letters*, v. 193, p. 423–436, doi:10.1016/S0012-821X(01)00509-X.
- Dumoulin, C., Choblet, G., and Doin, M., 2008, Convective interactions between oceanic lithosphere and asthenosphere: Influence of a transform fault: *Earth and Planetary Science Letters*, v. 274, p. 301–309, doi:10.1016/j.epsl.2008.07.017.
- Ebinger, C., and Sleep, N., 1998, Cenozoic magmatism throughout East Africa resulting from impact of a single plume: *Nature*, v. 395, no. 6704, p. 788–791, doi:10.1038/27417.
- Evans, J., and Achauer, U., 1993, Teleseismic velocity tomography using the ACH method: Theory and application to continental-scale studies, in *Seismic Tomography Theory and Practice*: London, Chapman and Hall, p. 319–360.
- Faccenna, C., Becker, T.W., Miller, M.S., Serpelloni, E., and Willett, S.D., 2014, Isostasy, dynamic topography, and the elevation of the Apennines of Italy: *Earth and Planetary Science Letters*, v. 407, p. 163–174, doi:10.1016/j.epsl.2014.09.027.
- Fantozzi, P., and Sgavetti, M., 1998, Tectonic and sedimentary evolution of the eastern Gulf of Aden continental margins: New structural and stratigraphic data from Somalia and Yemen, in Purser, B.H., and Bosence, D., eds., *Sedimentation and tectonics in rift basins: Red Sea-Gulf of Aden*: London, Chapman and Hall, p. 56–76.
- Ferguson, D.J., MacLennan, J., Bastow, I., Pyle, D., Jones, S., Keir, D., Blundy, J., Plank, T., and Yirgu, G., 2013, Melting during late-stage rifting in Afar is hot and deep: *Nature*, v. 499, no. 7456, p. 70–73, doi:10.1038/nature12292.
- Forte A.M., Quéré, S., Moucha, R., Simmons, N.A., Grand, S.P., Mitrovica, J.X., Rowley, D.B., 2010, Joint seismic–geodynamic–mineral physical modelling of African geodynamics: A reconciliation of deep-mantle convection with surface geophysical constraints: *Earth and Planetary Science Letters*, v. 295, p. 329–341.
- Frederiksen, A., Bostock, M., VanDecar, J., and Cassidy, J., 1998, Seismic structure of the upper mantle beneath the northern Canadian Cordillera from teleseismic travel-time inversion: *Tectonophysics*, v. 294, p. 43–55, doi:10.1016/S0040-1951(98)00095-X.

- Gerya, T.V., 2013, Three-dimensional thermomechanical modeling of oceanic spreading initiation and evolution: Physics of the Earth and Planetary Interiors, v. 214, p. 35–52, doi:10.1016/j.pepi.2012.10.007.
- Gurnis, M., Mitrovica, J., Ritsema, J., and Van Heijst, H., 2000, Constraining mantle density structure using geological evidence of surface uplift rates: The case of the African superplume: *Geochemistry, Geophysics, Geosystems*, v. 1, 1020, doi:10.1029/1999GC000035.
- Hansen, S.E., and Nyblade, A.A., 2013, The deep seismic structure of the Ethiopia/Afar hotspot and the African superplume: *Geophysical Journal International*, v. 194, p. 118–124, doi:10.1093/gji/ggt116.
- Hansen, S., Schwartz, S., Al-Amri, A., and Rodgers, A., 2006, Combined plate motion and density-driven flow in the asthenosphere beneath Saudi Arabia: Evidence from shear-wave splitting and seismic anisotropy: *Geology*, v. 34, p. 869–872, doi:10.1130/G22713.1.
- Hébert, H., Deplus, C., Huchon, P., Khanbari, K., and Audin, L., 2001, Lithospheric structure of the nascent west Gulf of Aden spreading center inferred from gravity data: *Journal of Geophysical Research*, v. 106, p. 26,345–26,363, doi:10.1029/2000JB900391.
- Immenhauser, A., 1996, Cretaceous sedimentary rocks on the Masirah Ophiolite (Sultanate of Oman): Evidence for an unusual bathymetric history: *Journal of the Geological Society (London)*, v. 153, p. 539–551, doi:10.1144/gsjgs.153.4.0539.
- Karato, S., 1993, Importance of anelasticity in the interpretation of seismic tomography: *Geophysical Research Letters*, v. 20, p. 1623–1626, doi:10.1029/93GL01767.
- Keen, C., 1985, The dynamics of rifting: Deformation of the lithosphere by active and passive driving forces: *Geophysical Journal International*, v. 80, p. 95–120, doi:10.1111/j.1365-246X.1985.tb05080.x.
- Kendall, J., Stuart, G., Ebinger, C., Bastow, I., and Keir, D., 2005, Magma-assisted rifting in Ethiopia: *Nature*, v. 433, no. 7022, p. 146–148, doi:10.1038/nature03161.
- Kennett, B., and Engdahl, E., 1991, Traveltimes from global earthquake location and phase identification: *Geophysical Journal International*, v. 105, p. 429–465, doi:10.1111/j.1365-246X.1991.tb06724.x.
- Kennett, B., Engdahl, E., and Buland, R., 1995, Constraints on seismic velocities in the Earth from traveltimes: *Geophysical Journal International*, v. 122, p. 108–124, doi:10.1111/j.1365-246X.1995.tb03540.x.
- Kennett, B., Sambridge, M., and Williamson, P., 1988, Subspace methods for large inverse problems with multiple parameter classes: *Geophysical Journal International*, v. 94, p. 237–247, doi:10.1111/j.1365-246X.1988.tb05898.x.
- King, S.D., and Anderson, D.L., 1998, Edge-driven convection: *Earth and Planetary Science Letters*, v. 160, p. 289–296, doi:10.1016/S0012-821X(98)00089-2.
- Korostelev, F., et al., 2014, Crustal and upper mantle structure beneath southwestern margin of the Arabian peninsula from teleseismic tomography: *Geochemistry, Geophysics, Geosystems*, v. 15, p. 2850–2864, doi:10.1002/2014GC005316.
- Lachenbruch, A.H., and Morgan, P., 1990, Continental extension, magmatism and elevation; formal relations and rules of thumb: *Tectonophysics*, v. 174, p. 39–62, doi:10.1016/0040-1951(90)90383-J.
- Leroy, S., et al., 2004, From rifting to spreading in the eastern Gulf of Aden: A geophysical survey of a young oceanic basin from margin to margin: *Terra Nova*, v. 16, p. 185–192, doi:10.1111/j.1365-3121.2004.00550.x.
- Leroy, S., et al., 2010a, Contrasted styles of rifting in the eastern Gulf of Aden: A combined wide-angle, multichannel seismic, and heat flow survey: *Geochemistry, Geophysics, Geosystems*, v. 11, Q07004, doi:10.1029/2009GC002963.
- Leroy, S., d'Acremont, E., Tiberi, C., Basuyau, C., Autin, J., Lucazeau, F., and Sloan, H., 2010b, Recent off-axis volcanism in the eastern Gulf of Aden: Implications for plume-ridge interaction: *Earth and Planetary Science Letters*, v. 293, p. 140–153, doi:10.1016/j.epsl.2010.02.036.
- Leroy, S., et al., 2012, From rifting to oceanic spreading in the Gulf of Aden: A synthesis: *Arabian Journal of Geosciences*, v. 5, p. 859–901, doi:10.1007/s12517-011-0475-4.
- Lucazeau, F., et al., 2008, Persistent thermal activity at the eastern Gulf of Aden after continental break-up: *Nature Geoscience*, v. 1, p. 854–858, doi:10.1038/ngeo359.
- Lucazeau, F., et al., 2009, Post-rift volcanism and high heat-flow at the ocean-continent transition of the eastern Gulf of Aden: *Terra Nova*, v. 21, p. 285–292, doi:10.1111/j.1365-3121.2009.00883.x.
- Lucazeau, F., Leroy, S., Rolandone, F., d'Acremont, E., Watremez, L., Bonneville, A., Goutorbe, B., and Düsünür, D., 2010, Heat-flow and hydrothermal circulation at the ocean-continent transition of the eastern Gulf of Aden: *Earth and Planetary Science Letters*, v. 295, p. 554–570, doi:10.1016/j.epsl.2010.04.039.
- Mechie, J., Ben-Avraham, Z., Weber, M., Götte, H.-J., Koulakov, I., Mohsen, A., and Stiller, M., 2013, The distribution of Moho depths beneath the Arabian plate and margins: *Tectonophysics*, v. 609, p. 234–249, doi:10.1016/j.tecto.2012.11.015.
- Molnar, P., and England, P., 1990, Late Cenozoic uplift of mountain ranges and global climate change: Chicken or egg? *Nature*, v. 346, no. 6279, p. 29–34, doi:10.1038/346029a0.
- Morency, C., Doin, M.-P., and Dumoulin, C., 2005, Three-dimensional numerical simulations of mantle flow beneath mid-ocean ridges: *Journal of Geophysical Research*, v. 110, B11407, doi:10.1029/2004JB003454.
- Moucha, R., and Forte, A.M., 2011, Changes in African topography driven by mantle convection: *Nature Geoscience*, v. 4, p. 707–712.
- Park, Y., Nyblade, A.A., Rodgers, A.J., and Al-Amri, A., 2007, Upper mantle structure beneath the Arabian Peninsula and northern Red Sea from teleseismic body wave tomography: Implications for the origin of Cenozoic uplift and volcanism in the Arabian Shield: *Geochemistry, Geophysics, Geosystems*, v. 8, Q06021, doi:10.1029/2006GC001566.
- Platel, J., and Roger, J., 1989, Evolution géodynamique du Dhofar (Sultanat d'Oman) pendant le Crétacé et le Tertiaire en relation avec l'ouverture du golfe d'Aden: *Bulletin de la Société Géologique de France*, ser. 8, v. 2, p. 253–263.
- Prell, W., et al., 1990, Neogene tectonics and sedimentation of the SE Oman continental margin: Results from ODP Leg 117, in Robertson, A.H.F., et al., eds., *The geology and tectonics of the Oman region: Geological Society of London Special Publication 49*, p. 745–758, doi:10.1144/GSL.SP.1992.049.01.45.
- Rawlinson, N., and Sambridge, M., 2005, The fast marching method: An effective tool for tomographic imaging and tracking multiple phases in complex layered media: *Exploration Geophysics*, v. 36, p. 341–350, doi:10.1071/EG05341.
- Rawlinson, N., Kennett, B., and Heintz, M., 2006, Insights into the structure of the upper mantle beneath the Murray Basin from 3D teleseismic tomography: *Australian Journal of Earth Sciences*, v. 53, p. 595–604, doi:10.1080/08120090600686751.
- Robinet, J., 2013, Evolution tectono-sédimentaire des marges orientale et méridionale de la plaque arabe (Sultanat d'Oman) [Ph.D. thesis]: Institut des Sciences de la Terre de Paris, Université Pierre et Marie Curie (Paris 6), 391 p.
- Robinet, J., Razin, P., Serra-Kiel, J., Gallardo-García, A., Leroy, S., Roger, J., and Grelaud, C., 2013, The Paleogene pre-rift to syn-rift succession in the Dhofar margin (northeastern Gulf of Aden): Stratigraphy and depositional environments: *Tectonophysics*, v. 607, p. 1–16, doi:10.1016/j.tecto.2013.04.017.
- Roger, J., Platel, J., Cavelier, C., and Bourdillon-de Grissac, C., 1989, Données nouvelles sur la stratigraphie et l'histoire géologique du Dhofar (Sultanat d'Oman): *Bulletin de la Société Géologique de France*, ser. 8, v. 2, p. 265–277.
- Rolandone, F., Lucazeau, F., Leroy, S., Mareschal, J.-C., Jorand, R., Goutorbe, B., and Bouquerel, H., 2013, New heat flow measurements in Oman and the thermal state of the Arabian Shield and Platform: *Tectonophysics*, v. 589, p. 77–89, doi:10.1016/j.tecto.2012.12.034.
- Rooney, T., Herzberg, C., and Bastow, I., 2012, Elevated mantle temperature beneath East Africa: *Geology*, v. 40, p. 27–30, doi:10.1130/G32382.1.
- Saltzer, R., and Humphreys, E., 1997, Upper mantle P wave velocity structure of the eastern Snake River Plain and its relationship to geodynamic models of the region: *Journal of Geophysical Research*, v. 102, p. 11,829–11,842, doi:10.1029/97JB00211.
- Saunders, A., Jones, S., Morgan, L., Pierce, K., Widdowson, M., and Xu, Y., 2007, Regional uplift associated with continental large igneous provinces: The roles of mantle plumes and the lithosphere: *Chemical Geology*, v. 241, p. 282–318, doi:10.1016/j.chemgeo.2007.01.017.
- Şengör, A.M.C., 2001, Elevation as indicator of mantle-plume activity, in Ernst, R.E., and Buchan, K.L., eds., *Mantle plumes: Their identification through time: Geological Society of America Special Paper 352*, p. 183–225, doi:10.1130/0-8137-2352-3.183.
- Sethian, J.A., 1996, A fast marching level set method for monotonically advancing fronts: *National Academy of Sciences Proceedings*, v. 93, p. 1591–1595, doi:10.1073/pnas.93.4.1591.
- Sethian, J.A., 1999, Level set methods and fast marching methods: Evolving interfaces in computational geometry, fluid mechanics, computer vision, and materials science (second edition): *Cambridge Monograph on Applied and Computational Mathematics 3*: Cambridge, Cambridge University Press, 404 p.
- Sethian, J.A., 2001, Evolution, implementation, and application of level set and fast marching methods for advancing fronts: *Journal of Computational Physics*, v. 169, p. 503–555, doi:10.1006/jcph.2000.6657.



- Sethian, J.A., and Popovici, A.M., 1999, 3-D traveltimes computation using the fast marching method: *Geophysics*, v. 64, p. 516–523, doi:10.1190/1.1444558.
- Shillington, D.J., Scott, C.L., Minshull, T.A., Edwards, R.A., Brown, P.J., and White, N., 2009, Abrupt transition from magma-starved to magma-rich rifting in the eastern Black Sea: *Geology*, v. 37, p. 7–10, doi:10.1130/G25302A.1.
- Sleep, N.H., 2002, Local lithospheric relief associated with fracture zones and ponded plume material: *Geochemistry, Geophysics, Geosystems*, v. 3, no. 12, 17 p., doi:10.1029/2002GC000376.
- Sobolev, S.V., Zeyen, H., Stoll, G., Werling, F., Altherr, R., and Fuchs, K., 1996, Upper mantle temperatures from teleseismic tomography of French Massif Central including effects of composition, mineral reactions, anharmonicity, anelasticity and partial melt: *Earth and Planetary Science Letters*, v. 139, p. 147–163, doi:10.1016/0012-821X(95)00238-8.
- Tard, F., Masse, P., Walgenwitz, F., and Gruneisen, P., 1991, The volcanic passive margin in the vicinity of Aden, Yemen: *Bulletin Centres Recherche Exploration–Production Elf-Aquitaine*, v. 15, p. 1–9.
- Tiberi, C., Leroy, S., d'Acremont, E., Bellahsen, N., Ebinger, C., Al-Lazki, A., and Pointu, A., 2007, Crustal geometry of the northeastern Gulf of Aden passive margin: Localization of the deformation inferred from receiver function analysis: *Geophysical Journal International*, v. 168, p. 1247–1260, doi:10.1111/j.1365-246X.2006.03294.x.
- Van Avendonk, H.J., Lavier, L.L., Shillington, D.J., and Manatschal, G., 2009, Extension of continental crust at the margin of the eastern Grand Banks, Newfoundland: *Tectonophysics*, v. 468, p. 131–148, doi:10.1016/j.tecto.2008.05.030.
- VanDecar, J., and Crosson, R., 1990, Determination of teleseismic relative phase arrival times using multi-channel cross-correlation and least squares: *Bulletin of the Seismological Society of America*, v. 80, p. 150–169.
- Watremez, L., Leroy, S., Rouzo, S., d'Acremont, E., Unternehr, P., Ebinger, C., Lucazeau, F., and Al-Lazki, A., 2011, The crustal structure of the northeastern Gulf of Aden continental margin: Insights from wide-angle seismic data: *Geophysical Journal International*, v. 184, p. 575–594, doi:10.1111/j.1365-246X.2010.04881.x.
- White, R., and McKenzie, D., 1989, Magmatism at rift zones: The generation of volcanic continental margins and flood basalts: *Journal of Geophysical Research*, v. 94, no. B6, p. 7685–7729, doi:10.1029/JB094iB06p07685.
- White, R., et al., 2008, Lower-crustal intrusion on the North Atlantic continental margin: *Nature*, v. 452, no. 7186, p. 460–464, doi:10.1038/nature06687.
- Whitmarsh, R., 1979, The Owen Basin off the south-east margin of Arabia and the evolution of the Owen Fracture Zone: *Geophysical Journal International*, v. 58, p. 441–470, doi:10.1111/j.1365-246X.1979.tb01034.x.